*International Journal of Engineering Science Invention (IJESI)*
*ISSN (Online): 2319-6734, ISSN (Print): 2319-6726*
*www.ijesi.org ||Volume 11 Issue 8August 2022 || PP 34-48*

# 1.75 eV Bright Red Emission of $Pr^{3+}$ ions doped in CaO-PbO-$B_2O_3$-$SiO_2$ glasses by $Fe^{3+}$ sensitizer ions for red laser and LED

K. Kalyan Chakravarthi and M. Rami Reddy*
*Department of Physics, Acharya Nagarjuna University, Nagarjuna Nagar-522503, India.*

***ABSTRACT:*** *$Pr_2O_3$ and $Fe_2O_3$ Co-doped with synthesized composition (in mol%) of 20 CaO – (29-x) PbO– 25 $B_2O_3$ –25$SiO_2$ by conventional melt-quenching technique. The Optical absorption spectra contains eight absorption transitions in vis-NIR regions due to presence of $Pr^{3+}$ ions. The visible spectra also exhibited a weak transition at about 440 nm was identified being due to $^6A_{1g}$ ($^6S$) $\rightarrow$$^4T_{2g}$ ($^4G$) ($O_6$) absorption transition of $Fe^{3+}$ ions. The PL spectra of Fe contained glasses were exhibited a peak at about 711 nm characteristic octahedral emission transition of $Fe^{3+}$ ions. The $Pr^{3+}$-$Fe^{3+}$ co-doped glasses exhibited several emission transitions due to presence of $Pr^{3+}$ ions. Among all the emission transitions, $^3P_0\rightarrow^3F_2$ and $^3H_6$ are identified to be prominent emission transitions. While gradual increase of $Fe_2O_3$ mol%, the transition intensity of $^3P_0\rightarrow^3F_2$ were found to be increased many folds with respect to that of $Fe^{3+}$ ions free glass. From the quantitative analysis of these results there is a gradual increase in the efficient energy transfer from octahedral $Fe^{3+}$ ions to $Pr^{3+}$ions ($Fe^{3+}\rightarrow Pr^{3+}$) when the mol% is 1.0. Finally, it is concluded that the preferable 1 .0 mol% of $Fe_2O_3$ for getting highest efficient luminescence of $Pr^{3+}$ ions in Bright Red of 1.75 eV.*

***KEYWORDS-****Borosilicate glasses, EPR, FTIR, Luminescence spectra, Optical absorption.*

---

Date of Submission: 12-08-2022 Date of Acceptance: 28-08-2022

---

## I. INTRODUCTION

Oxide glasses (Borosilicate) have high photon energy (1100 $cm^{-1}$) due to the stretching vibrations of network forming $SiO_2$ and $B_2O_3$ oxides. Borosilicate glasses have several features such as high transmission property, highly chemical resistant, excellent light glasses, low thermal expansion and high chemical durability. Borosilicate glasses have wide range applications such as LCD, Touch Screens, Opto-caps in laser diodes and solar cells. Lead Borosilicate (PbBSi) glasses have extensive glass formation range and low melting temperature at ~950$^oC$. Low melt temperature of glasses such as lead borosilicate glasses (PbBSi) are of interest for application in Nuclear waste Immobilization [1, 2]. Nowadays, Heavy Metal Oxides (HMO) glasses have attracted much attention for photonic and radiation shielding applications due to outstanding physical and Optical properties [3, 4]. At low mol% (below 40%) PbO acts as network modifier in borosilicate glass and to form high stable glasses, enriching linear and non-linear refractive indexes due to its low field strength and high polarizability [5]. Glasses containing HMO (PbO) are excellent applications in non-linear optical instruments [6]. Bonding oxygens (BO) linkers among main building-blocks of the glass structure oxide based inorganic glasses exhibit in addition of unique feature like transparent in visible light. Alkali earth oxide with large size, low valency cations do not act as glass formers.

Glasses containing TM ions contributed to fiber optic communications, luminescent, solar energy concentrations, memory module and photo conducting devices [7]. Light Rare Earth Elements (Lanthanides-Ln) originated most stable oxidation state of +3 ($Ln^{3+}$). Light Rare Earth Elements are applicable in UV-absorber and Anti-browning agents. Praseodymium used in production of Atomic Batteries. Glasses containing Rare Earth ions ($RE^{n+}$) are authenticating to be luminescent materials as they have high emission efficiencies. Rare Earth ions emissions correspond to 4f-4f electronic transitions. Glasses Confined with $RE^{3+}$ ions has increased hardness and a higher elastic module and chemical durability [8]. Glasses doped with $RE^{3+}$ ions to form transitions in the glasses with intra $4f^2$ electronic transition and exhibit several sharp lines in the UV-vis region and near IR owing to the shielding effects of 5s and 5p orbitals [9, 10].

In recent years a large number of amorphous host materials are co-doped with TM and RE ions are extensively used for the study of structure and local symmetry of the materials for high potential application for different fields. Glasses collaborated with $Fe_2O_3$ are applicable in electrochemical, electronic and electro-optic devices [11, 12]. The addition of $Fe_2O_3$ (below1 mol%) most commonly used coloring components in borosilicate glasses [13]. Calcium Lead Borosilicate glasses mixed with RE and TM ions are the main subject of

research field because of their outstanding optical and physical properties. In modern days, Alkali earth heavy metal borosilicate oxide glasses like CaO-PbO-$B_2O_3$-$SiO_2$ glasses have excellent various technological application.

The extensively Co-doping technique used for TMO and REE for modifying structural, physical and spectroscopic properties in calcium lead borosilicate glasses. In this study, calcium lead modified borosilicate glasses were selected to be doped with rare earth metal oxide and transition metal oxide hoping to alter produce unique absorption and emission profile. In the present paper, our objective is to investigate the spectroscopic and structural modification in calcium lead borosilicate glasses co-doped with $Pr_2O_3$ and $Fe_2O_3$ are undertaken.

## II. SYNTHESIS REACTION OF GLASSES

For novel glass system, the chemical substances such as $SiO_2$+$B_2O_3$, CaO, PbO, $Pr_2O_3$ and $Fe_2O_3$ are engaged in the chemical combination reaction. The synthesis reaction of the new glass system is performed in Fig.1.

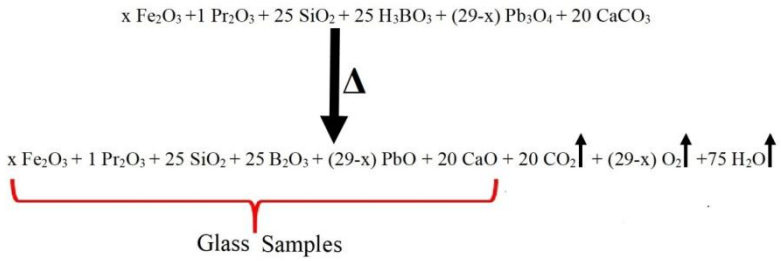


Figure 1: synthesis reaction of glasses

## III. Experimental Procedure

A Novel series of glass compositions of 20 CaO – (29-x) PbO – 25 $B_2O_3$ – 25 $SiO_2$: 1$Pr_2O_3$ + x $Fe_2O_3$ (where 'x' varies from 0 to 1 mol% with increasing step of 0.2 mol%) were prepared by conventional melt quenching process. Commercial chemicals of AR-grade (99.9% of purity) of CaO, PbO, $SiO_2$, $B_2O_3$, $Pr_2O_3$ and $Fe_2O_3$ are appropriate amounts of chemicals are weighed and powdered in the composition ratios. Agate mortar and pestle grinded to obtain homogeneous glass mixture for melt quenching process about an hour. The glass composition powders are transferred to a 50 ml silica crucible is used to melt finely mixed powders of chemicals with an electric programmable furnace. The glasses were melt at 974 $^oC$ for nearly 25 minutes. In electric furnace, the silica crucible comprising the melt was occasionally swirled in the furnace for a few minutes to obtain homogenize the glass melt. The melt is then quenched at room temperature in air to form a required glasses. These glass samples instantly transferred to another furnace previously kept at 420 $^oC$ and annealed at this temperature for 5 hours to remove thermal stresses generated by slow cooling. All glass samples were made in required shapes. The glass samples were polished with different grades of emery powder for UV-visible-NIR spectroscopic measurements. The glass compositions are given in Table 1.

TABLE 1: Novel Glass Composition of CaO-PbO-$B_2O_3$-$SiO_2$:$Pr^{3+}$/ $Fe^{3+}$Co-doped Glasses

| S. No | Glass Codes | CaO mol% | PbO mol% | $B_2O_3$ mol% | $SiO_2$ mol% | $Pr_2O_3$ mol% | $Fe_2O_3$ mol% |
|---|---|---|---|---|---|---|---|
| 1 | Pr | 20 | 29 | 25 | 25 | 1 | - |
| 2 | PrFe0.2 | 20 | 28.8 | 25 | 25 | 1 | 0.2 |
| 3 | PrFe0.4 | 20 | 28.6 | 25 | 25 | 1 | 0.4 |
| 4 | PrFe0.6 | 20 | 28.4 | 25 | 25 | 1 | 0.6 |
| 5 | PrFe0.8 | 20 | 28.2 | 25 | 25 | 1 | 0.8 |
| 6 | PrFe1.0 | 20 | 28 | 25 | 25 | 1 | 1.0 |

Hereafter the host glass coded as CaPbBSi and other glasses coded as Pr, PrFe0.2, PrFe0.4, PrFe0.6, PrFe0.8, PrFe1.0 glass systems are prepared at melting temperature as 965, 967, 968, 970, 974 and 974 $^oC$ respectively. Fig.2 shows the prepared transparent CaO-PbO-$B_2O_3$-$SiO_2$: $Pr^{3+}$ - $Fe^{3+}$ co-doped glasses. The color of the glass samples changes from bluish to thick brown with increasing mol% $Fe_2O_3$ content.


Figure 2:CaO-PbO-$B_2O_3$-$SiO_2$:$Pr^{3+}$/ $Fe^{3+}$ Co-doped glass samples

3.1 Sample Characterization

The mass of the samples are recorded using a scale tech weighing balance. Scale Tech digital weighing balance with a precision of $10^{-4}$ gm/cm$^3$ recorded the weight of the glasses. The weights of the glasses were used to obtain the density values using Archimedes' technique. The Refractive index of these glass samples were measured by using Abbe's Refractometer. The Optical absorption (UV-Vis-NIR) spectra was recorded JASCO, V-570 spectrophotometer from 200 to 2500 nm with an accuracy of 0.1 nm. The ESR spectra of powder samples were recorded at room temperature using E11Z Varian X band (T=9.5GHz) of ESR spectrometer of 100 kHz field modulation. The X-ray diffraction patterns of the samples are recorded using a Shimadzu XRD-7000. FTIR spectra were recorded on a JASCO-FTIR-140 spectrophotometer with resolution of 0.2 cm$^{-1}$. The spectral range is from 400 to 4000 cm$^{-1}$ using KBr pellets (300 mg) containing the pulverized sample (1.5 mg) and the spectra was analyzed in the range of 400 to 2000 cm$^{-1}$. The photoluminescence spectra was recorded at room temperature on a Photon Technology International spectroflurometer (PTI) with excited wavelength ($\lambda_{excitation}$) 482 nm from 300 to 900 nm.

## IV. Results

4.1 Physical Properties

The evaluated values of Average molecular weights, densities, refractive indices, molar refractivity's, Polaron radius, oxygen packing density's and some other parameters of the $Pr^{3+}$ - $Fe^{3+}$ ions co-doped CaPbBSi glass systems are given in Table 2.

TABLE 2: Various Physical Properties of CaO-PbO-$B_2O_3$-$SiO_2$ : $Pr^{3+}$/ $Fe^{3+}$Co-doped Glasses

| Physical Properties | Pr | PrFe0.2 | PrFe0.4 | PrFe0.6 | PrFe0.8 | PrFe1.0 |
|---|---|---|---|---|---|---|
| Thickness **(t)**(mm) (±0.001) | 1.452 | 1.451 | 1.213 | 1.125 | 1.265 | 1.151 |
| Density ***(ρ)*** (gm/cm$^3$) (± 0.004) | 4.8002 | 4.7916 | 4.7891 | 4.7745 | 4.7660 | 4.7574 |
| Average Molecular Weight ***(M)***(g/mol) | 111.61 | 111.48 | 111.36 | 111.23 | 111.02 | 110.98 |
| Transition Metal Ion Concentration $(N_i)$($10^{22}$ ions/cm$^3$) (± 0.005) | -- | 0.5178 | 1.0352 | 1.5529 | 2.0683 | 2.5841 |
| Inter transition metal ion distance $(R_i)$ (Å) (± 0.005) | -- | 5.7802 | 4.5883 | 4.0082 | 3.6432 | 3.3825 |
| Polaron radius $(R_p)$**(Å)**(± 0.005) | -- | 2.3294 | 1.8491 | 1.6153 | 1.4682 | 1.3631 |
| Field strength $(F_i)$ ($10^{15}$ cm$^{-2}$) (± 0.005) | -- | 5.5307 | 8.7741 | 11.4978 | 13.9175 | 16.1461 |
| Electronic polarizability $(\alpha_e)$ ($10^{-23}$ ions/cm$^3$) (± 0.005) | -- | 1.7327 | 0.8679 | 0.5796 | 0.4358 | 0.3489 |
| Molar Volume $(V_m)$ (x $10^{14}$ cm$^3$ mol$^{-1}$) | 23.2511 | 23.2657 | 23.2820 | 23.2967 | 23.3115 | 23.3279 |
| Refractive index $(\mu)$ (± 0.0001) | 1.6641 | 1.6752 | 1.6764 | 1.6779 | 1.6795 | 1.6796 |
| Refraction losses | 0.2203 | 0.2252 | 0.2257 | 0.2264 | 0.2271 | 0.2272 |
| Molar Refractivity $(R_M)$ (± 0.0005) | 8.6253 | 8.7437 | 8.7619 | 8.7828 | 8.8042 | 8.8118 |
| Dielectric Constant $(\varepsilon)$(± 0.0005) | 2.7692 | 2.8063 | 2.8103 | 2.8154 | 2.8207 | 2.8211 |
| Specific Volume $(V_s)$ | 0.2084 | 0.2087 | 0.2091 | 0.2095 | 0.2098 | 0.2111 |
| Optical Dielectric Constant $(\varepsilon_o)$ | 1.7692 | 1.8063 | 1.8103 | 1.8154 | 1.8207 | 1.8211 |
| Oxygen Packing Density **(OPD)** | 80.914 | 80.712 | 80.576 | 80.411 | 80.316 | 80.247 |
| Optical Basicity$(\Lambda_{th})$ | 0.7611 | 0.7628 | 0.7639 | 0.7645 | 0.7654 | 0.7662 |

4.2 Power X-Ray Diffraction Studies

The X-ray diffraction angles are taken an accuracy of ± 0.1$^o$ lines. Two broad bumps were observed at around ~30$^o$ and ~48$^o$ (=2θ) without sharp peaks. The analysis suggests glassy behavior of the sample. Sharp Peak free

from X-ray spectra confirmed that the amorphous nature of all the glasses. This analysis suggest glassy character of the glass samples. Fig.3shows the X-ray diffraction patterns of CaO-PbO-$B_2O_3$-$SiO_2$ : $Pr^{3+}$ / $Fe^{3+}$ co-doped glasses.

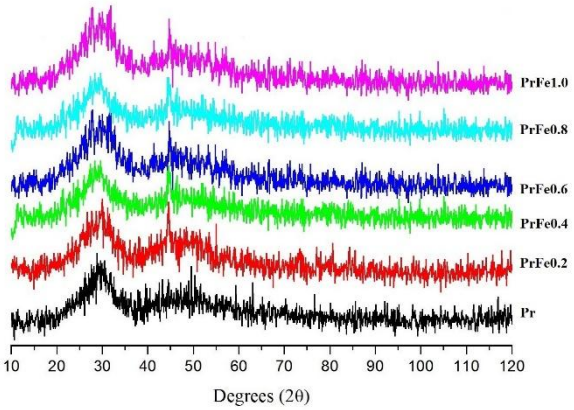


Figure 3: X-ray diffraction patterns of CaO-PbO-$B_2O_3$-$SiO_2$: $Pr^{3+}$/$Fe^{3+}$ Co-doped glasses

4.3 Differential Thermal Analysis

The thermal stability glass defined as the temperature range of the glass more precisely under cooled melt to draw into fiber. The Fig.4 shows DTA curves for Pr, PrFe0.6 and PrFe1.0 glasses. From the Fig.4 it was observed that the glass transition temperature ($T_g$), glass crystallization temperature ($T_c$) and glass melting temperature ($T_m$) of these glasses are given in Table 3.

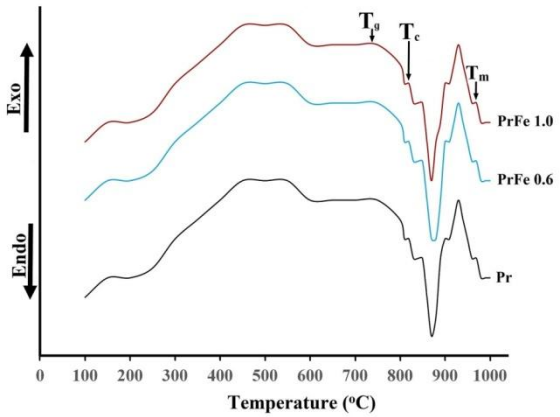


Figure 4: DTA curves of CaO-PbO-$B_2O_3$-$SiO_2$: $Pr^{3+}$/$Fe^{3+}$ Co-doped glasses

The thermal stability factor is $\Delta T=T_c-T_g$ is the difference between glass crystallization temperature ($T_c$) and glass transition temperature ($T_g$). Each hump is assigned to the glass transition temperature ($T_g$), crystallization temperature ($T_c$) and melting temperature ($T_m$) respectively. From DTA Spectra it was observed that $T_g$ depends on the strength of chemical bonds in the glass structure. Hruby's Parameter gives the information on the stability of the glass against devitrification. The stability of the glass in order of PrFe1.0 > PrFe0.6 > Pr. Table.3 indicates PrFe1.0 glass are highly stable against devitrification.

TABLE 3: Values of glass transition temperature ($T_g$), crystallization temperature ($T_c$), melting temperature ($T_m$), Thermal Stability ($\Delta T$) and Hruby's Parameter of various glass samples

| Glass Sample Code | Glass Transition Temp ($T_g$) °C | Glass Crystallization Temp ($T_c$) °C | Glass Melting Temp ($T_m$) °C | Thermal Stability ($\Delta T=T_c-T_g$) °C | Hruby's Parameter |
|---|---|---|---|---|---|
| Pr | 749 | 841 | 965 | 96 | 0.7442 |
| PrFe0.6 | 748 | 843 | 970 | 95 | 0.7480 |
| PrFe1.0 | 744 | 845 | 974 | 97 | 0.7823 |

4.4 EDS Analysis

The Energy Dispersive Spectroscopy the chemical compositions of the glasses were determined and shown in Fig.5. The Fig.5 shows the Energy Dispersive Spectroscopy of the glass samples of 1 mol% of CaO-PbO-$B_2O_3$-$SiO_2$ : $Pr^{3+}$ - $Fe^{3+}$ions co-doped glasses.

This analysis indicates the presence of calcium (Ca), silicon (Si), boron (B), lead (Pb), oxygen (O), praseodymium (Pr) and iron (Fe) elements in the glass network.

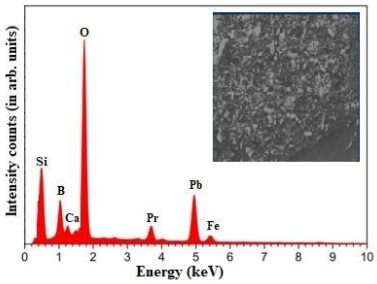


Figure 5: EDS of CaO-PbO-$B_2O_3$-$SiO_2$: $Pr^{3+}$ / $Fe^{3+}$Co-doped glasses

4.5 FTIR Spectra

Fourier Transmission-infrared spectra of $Pr^{3+}$ - $Fe^{3+}$ ions co-doped CaO-PbO-$B_2O_3$-$SiO_2$ glasses are recorded at room temperature (37 $^oC$) exhibited large, medium, weak and different bands due to the structural vibration modes of Silicate, borate and borosilicate functional groups as shown in Fig.6.

According to the lead borosilicate literature survey, the structural vibrations of borosilicate groups are mainly present in the following spectral regions are ($\nu_1$) the region at 430 $cm^{-1}$ due to the Combined Vibrations of $BO_4$ and $PbO_4$ units, ($\nu_2$) the region at 480 $cm^{-1}$due to the Symmetrical Bending Vibrations of Si–O–Si linkage, ($\nu_3$) the region at 695 $cm^{-1}$ due to the Bending Vibrations of B-O-B due to $BO_3$ and $BO_4$ structural units, ($\nu_4$) the region at 860 $cm^{-1}$ due to the Stretching Vibrations B–O bond of the $BO_4$ tetrahedral units, ($\nu_5$) the region at 910 $cm^{-1}$ due to the Stretching Vibrations of B–O–Si linkage units, ($\nu_6$) the region at 1090 $cm^{-1}$ due to the Asymmetrical bending vibrations of Si–O–Si and ($\nu_7$) the region at 1410 $cm^{-1}$ due to the Symmetric stretching relaxation of the B–O band of trigonal $BO_3$ units. The summary of data on the spectra band positions in the FT-IR spectra of $Pr^{3+}$ - $Fe^{3+}$ ions co-doped CaO-PbO-$B_2O_3$-$SiO_2$ glasses are presented in Table 4.

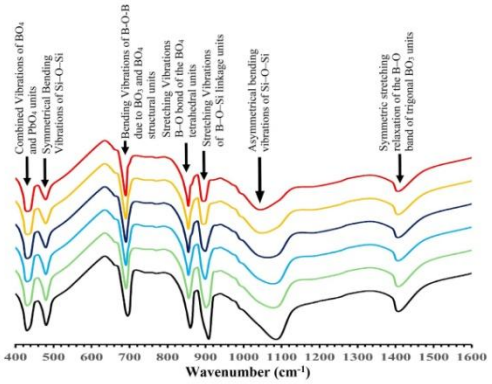


Figure 6: FTIR spectra of CaO-PbO-$B_2O_3$-$SiO_2$:$Pr^{3+}$ / $Fe^{3+}$ Co-doped glasses

TABLE 4: FT-IR spectra band positions CaO-PbO-$B_2O_3$-$SiO_2$:$Pr^{3+}$/ $Fe^{3+}$Co-doped glasses

| Band Positon | Glass Samples | | | | | | Band Assignments |
|---|---|---|---|---|---|---|---|
| | Pr | PrFe0.2 | PrFe0.4 | PrFe0.6 | PrFe0.8 | PrFe1.0 | |
| 1 | 430 | 428 | 431 | 430 | 430 | 430 | Combined Vibrations of $BO_4$ and $PbO_4$ units |
| 2 | 480 | 481 | 480 | 482 | 480 | 480 | Symmetrical Bending Vibrations of Si–O–Si |
| 3 | 695 | 694 | 694 | 695 | 694 | 695 | Bending Vibrations of B-O-B due to $BO_3$ and $BO_4$ structural units |
| 4 | 860 | 861 | 862 | 860 | 862 | 860 | Stretching Vibrations B–O bond of the $BO_4$ tetrahedral units |
| 5 | 910 | 911 | 911 | 911 | 912 | 910 | Stretching Vibrations of B–O–Si linkage units |
| 6 | 1090 | 1092 | 1091 | 1091 | 1094 | 1090 | Asymmetrical bending vibrations of Si–O–Si |
| 7 | 1410 | 1411 | 1410 | 1410 | 1410 | 1410 | Symmetric stretching relaxation of the B–O band of trigonal $BO_3$ units |

4.6 Optical Absorption Spectra

An Optical absorption spectra of $Pr^{3+}$ - $Fe^{3+}$ co-doped CaO-PbO-$B_2O_3$-$SiO_2$ glasses in the wavelength range between 200 to 2500 nm at RT is shown in Fig.7. This Optical absorption spectra exhibits eight absorption transitions corresponding to the intra $4f^2$-configuration and electric dipole transitions of $Pr^{3+}$ ions. All the transition in the absorption spectrum are started from the ground level ($^3H_4$) to various exited levels $^3P_{2,\,1,\,0}$ , $^1D_2$, $^1G_4$, $^3F_{4,\,3,2}$ and $^3H_{6,5}$ responsible for $Pr^{3+}$ species in the glass matrix [14, 15].

The iconic hump absorption transition for $Pr^{3+}$ ions: $^3H_4 \rightarrow {}^3P_2$ (at 440 nm), $^3H_4 \rightarrow {}^3P_1$ (at 467 nm), $^3H_4 \rightarrow {}^3P_0$ (at 482 nm), $^3H_4 \rightarrow {}^1D_2$ (at 591 nm), $^3H_4 \rightarrow {}^1G_4$ (at 1011 nm), $^3H_4 \rightarrow {}^3F_4$ (at 1426 nm), $^3H_4 \rightarrow {}^3F_3$ (at 1525 nm) and $^3H_4 \rightarrow {}^3F_2$ (at 1938 nm). $^3H_4 \rightarrow {}^3P_{2,\,1,\,0}$ and $^1D_2$ are originated in visible region. $^3H_4 \rightarrow {}^3F_{4,\,3,\,2}$ and $^3H_4 \rightarrow {}^1G_4$ are identified at infra-red region. V. Naresh and S. Buddhudu reported that the optical absorption spectra containing $Fe_2O_3$ glasses, it was attributed to the d-d transitions of $^6A_{1g}$ ($^6S$) $\rightarrow {}^4T_{2g}$ ($^4G$) band associated at 456 nm in the visible region indicates the iron ions present in the trivalent state (Ferric ions) [16].

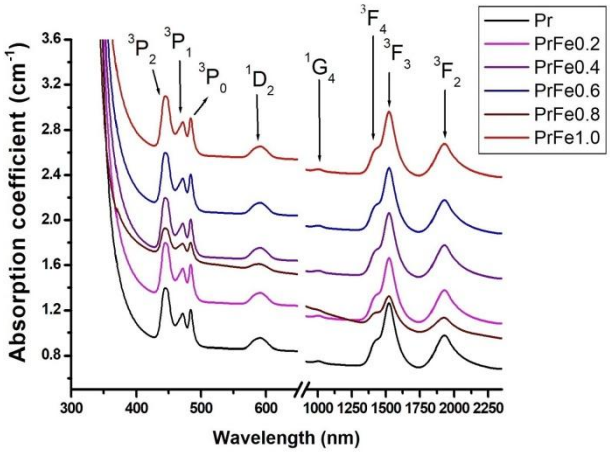


Figure 7: Optical absorption spectra of CaO-PbO-$B_2O_3$-$SiO_2$: $Pr^{3+}$/ $Fe^{3+}$ Co-doped glasses

In the present article, we also recorded UV-Visible spectra of glass system containing 1 mol% of $Fe_2O_3$ without $Pr_2O_3$ as shown in Fig.8. From the Fig.8 it was observed that 1 mol% of $Fe_2O_3$ doped CaPbBSi shows a weak absorption transition $^6A_{1g}$ ($^6S$) $\rightarrow {}^4T_{2g}$ ($^4G$) band at 440 nm. The transition $^6A_{1g}$ ($^6S$) $\rightarrow {}^4T_{2g}$ ($^4G$) related to the $Fe^{III}$ ions in octahedral ($O_6$) coordination [17, 18].

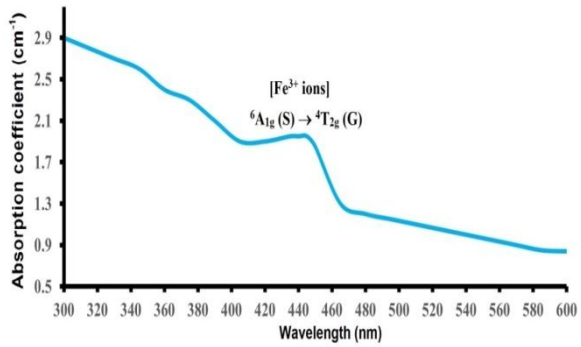


Figure 8: Optical Absorption spectra of $Fe_2O_3$ doped CaO-PbO-$B_2O_3$-$SiO_2$ glass

From the Fig.7 it was found that increasing mol% of $Fe_2O_3$ in the glass system the $^6A_{1g}$ ($^6S$) $\rightarrow$$^4T_{2g}$ ($^4G$) band is seems to be exactly merged with $^3H_4\rightarrow{}^3P_2$ absorption band of $Pr^{3+}$ species.

4.7 Electron Paramagnetic Resonance Spectra

No EPR Resonance signal was detected in the spectra of un-doped glasses indicates that there is no paramagnetic impurities. The EPR Resonance signals of $Pr^{3+}$ - $Fe^{3+}$ cations co-doped in CaO-PbO-$B_2O_3$-$SiO_2$ glasses at room temperature (37 $^oC$) given in Fig. 9. From the Figure.9 it was observed that the intensities of EPR lines are increasing with increasing concentration of $Fe_2O_3$ in the glass system. Introduction of $Fe^{3+}$- $Pr^{3+}$ cations into CaPbBSi co-doped glasses with different mol% (0.2, 0.4, 0.6, 0.8 and 1.0 mol%) investigates glass samples exhibits intense EPR signals. The intense resonance signal-I at g≈2.00 (centered and weak signal) and additionally an intensive of sharp line signal-II at g≈4.384 (157.5 mT) is due to isolated $Fe^{3+}$ ions predominantly located in octahedral sites ($O_6$) and along with broad signal-III (at left shoulder) at g≈9.37 (77.5 mT).

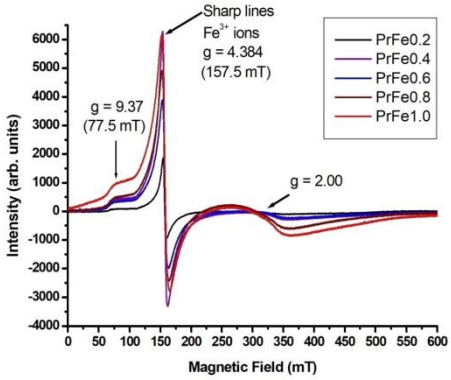


Figure 9: EPR spectra of CaO-PbO-$B_2O_3$-$SiO_2$ : $Pr^{3+}$ / $Fe^{3+}$ Co-doped glasses

4.8 Photoluminescence Spectra (PL)

CaO-PbO-$B_2O_3$-$SiO_2$ glass host co-doped with $Pr^{3+}$ - $Fe^{3+}$ ions as shown in Fig.10. The room temperature of Photoluminescence (PL) spectra was recorded with an excitation wavelength ($\lambda_{exe}$) of 482 nm. The PL spectra of CaPbBSi glasses containing $Pr^{3+}$ species exhibits several emission transitions which are denoted as $^3P_0\rightarrow{}^3H_4$ (at 455 nm), $^3P_1\rightarrow{}^3H_5$ (at 510 nm), $^3P_0\rightarrow{}^3H_5$ (at 552 nm), $^1D_2\rightarrow{}^3H_4$ (at 612 nm), $^3P_0\rightarrow{}^3H_6$ (at 656 nm), $^3P_0\rightarrow{}^3F_2$ (at 711 nm) and$^3P_1\rightarrow{}^3F_3$ (at 750 nm) from the emission transition literature of $Pr^{3+}$ species [15]. Amit Kumar Prasad and Mayank Jain researches investigated and confirmed that the emission spectra of $Fe^{3+}$ ions exhibited a band around at 729 nm associated to the transition of $^4T_{2g}$ ($^4G$) $\rightarrow{}^6A_{1g}$ ($^6S$) [19]. While increasing strength of $Fe_2O_3$ in glass system the hyper sensitive emission transition is observed at 711 nm in PL emission spectra.

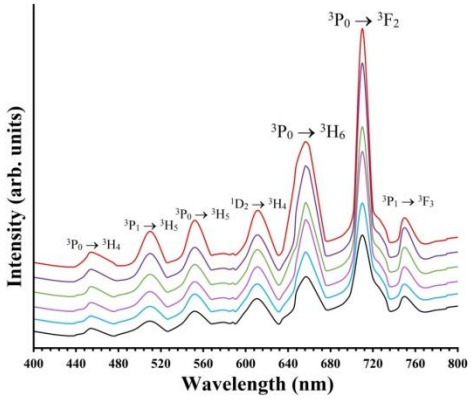


Figure 10: PL spectra of CaO-PbO-$B_2O_3$-$SiO_2$ : $Pr^{3+}$ / $Fe^{3+}$ Co-doped glasses

## V. Discussions

The network formers which constitutes the back bone of the glass structure. The structure of borosilicate glasses are mixed three dimensional (3D) complexes. $SiO_2$ and $B_2O_3$ chemicals are non-metallic oxides and forms $Si^{4+}$ and $B^{3+}$ non-metallic small cations. In borosilicate glasses $SiO_2$ and $B_2O_3$ mix together to form covalent bonds. $SiO_2$ and $B_2O_3$ are traditional and outstanding glass formers and $SiO_4$ is the basic building structural unit of silicate in borosilicate glasses. Borosilicate glasses containing $SiO_4$ and $BO_4$ structural units fuse to form borosilicate long chains. Oxide ions ($O^{2-}$) acts as bridges between the structural units, they are called bridging oxygens (BO). The formation of bridging oxygens (BO) depends on the glass composition and structure of the glass. The addition of CaO in the glass, the transition contributes to the production of meta, pyro and ortho-silicates in order $[SiO_{4/2}]^o$ ($Q^o$), $[SiO_{3/2}\,O]^{-1}$ ($Q^1$), $[SiO_{2/2}\,O_2]^{-2}$ ($Q^2$), $[SiO_{1/2}\,O_3]^{-3}$ ($Q^3$) and $[SiO_4]^4$ ($Q^4$) and CaO (alkali earth oxide) depolymerizing in silicate network.

$$2\,[SiO_4]^{\,o} + CaO \rightarrow 2\,[SiO_{1/2}\,O_3]^{-3} + Ca^{2+}$$

$Ca^{2+}$ cations plays a role in charge-balancer of the $SiO_{4/2}$ and $Ca^{2+}$ big cations accumulated around structural units due to negative charge localization. $B_2O_3$ is binary glass former in borosilicate glass have two dimensional (2D) layout structure with triangle $BO_3$ ($B_3$) and tetrahedral $BO_4$ ($B_4$) structural units participated in silicate network depending on the glass composition. The introduction of modifier HMO (PbO) enters in the borate network of borosilicate layout by forming 4-fold $BO_4$ with forming NBOs.

$$2\,[BO_3] + PbO \rightarrow 2\,[BO_4]^- + Pb^{2+}$$

Addition of PbO modifier in borosilicate layout the $PbO_4$ structural units helps conversion of $[BO_3]\rightarrow[BO_4]$ structural units by forming more $BO_4$ ($B_4$) structural units with non-bridging oxygens (NBOs) and depolymerizing in borate layout. Modifier plumbous ($Pb^{2+}$) cations connect with bridging oxygens (BO) in the borate network. The modifier anions are more randomly distributed in the borosilicate network. Borosilicate glass layout borate and silicate structural units in the layout strongly interact without PbO modifier with its structural unit $PbO_4$. Therefore, the varying PbO content in the borosilicate network the increasing $B_4$ structural units. In borosilicate glasses, the effect of silica on the boron –oxygen coordination and the possible inter-tetrahedral avoidance that exist between $BO_4$ and $SiO_4$ structural units. The addition of mol% of network modifiers to modify the properties of glasses. The addition of network modifiers breaks the glass network and leads to the creation of non-bridging oxygens (NBOs) and are connected to the network only at one end. The 4-fold $BO_4$ entities dominate in the silicate-rich domain, whereas 3-fold boron entities prevail in the borate-rich hand and forms easily B-O-Si (Borosilicate Bridge) linkage. Each $SiO_4$ structural unit linked with one $SiO_4$ one $BO_4$ structural units and one oxygen from each unit linked with a metal ion and leads the structure formation of long tetrahedral (4-fold) chains [20, 21].

Density physical parameter of the glass is the fundamental key to analyze various spectroscopic properties like optical band gap and structural compactness. Refractive index is binary key physical parameter to evaluate the oxygen packing density and formation of NBOs in the glass system. Decreasing density with decreasing trend in optical direct and indirect band gaps energy by increasing concentration of $Fe_2O_3$ in the glass layout. Increasing quite trend in Urbach Energy ($\Delta E$) verses increasing refractive index of glasses is observed with increasing mol% of $Fe_2O_3$. The increasing Transition Metal ion Concentration ***($N_i$)*** influence the variation intensity of ESR spectra of co-doped glassy network. The structural compactness of glasses is observed from physical parameters like Polaron radius, field strength, molar volume and electronic polarizability values. High Optical basicity value of glasses means distribution of oxide ions ($O^{2-}$) in the prepared glass environment. While, Optical basicity increasing with increasing $Fe_2O_3$ content means a high-rich electron donor ability of oxide ions ($O^{2-}$) in the glassy environment. The physical parameters density and molar volume of glasses are

observed in quite reverse trend that indicating change in the geometrical configuration of glassy network. Physical parameters of all glasses are evaluated and strongly influenced the variation of NBOs, electron density carried by oxygen and optical band gap in the glasses with varying $Fe_2O_3$ content.

FT-IR is a technical tool, to study molecular structure modifications in local environments in the glass system. Silicon exhibits catenation property to form inorganic long chains and 4-fold coordination like carbon element. $SiO_4$ structural units as a series of isolated silicon atoms like silicons. In borosilicate glasses silicon, boron and oxygen are the backbone of the borosilicate network. In borosilicate glasses the fundamental building structural units are 4-fold coordinated $SiO_4$ and $BO_4$ units. Silica and boric acid are typical non-metal and forms only covalent bonds to form more NBOs in the glass network. Silica and boric acid instantly react with more electropositive elements like $Ca^{2+}$ and $Pb^{2+}$ to form bonding oxygens like NBOs in the glass network. In borosilicate glasses the silicates, borates together originating to form different network linkages. Raw silicones were mixed together to create NBOs in the glass matrices. The NBOs in the glass system gets evenly distributed TMO and RMO.

The FTIR vibrational spectra of CaO-PbO-$B_2O_3$-$SiO_2$: $Pr^{3+}$- $Fe^{3+}$ ions co-doped glasses exhibits different modes of bands with their structural vibrations. The first band ($\nu_1$) at 430 $cm^{-1}$ originated due to the combined vibrations of $BO_4$ and $PbO_4$ structural units [22], the second band ($\nu_2$) at 480 $cm^{-1}$ is due to the Symmetrical Bending Vibrations of ≡Si-O-Si≡ (strong and di-silicate linkage) associated with two $SiO_4$ structural units connected by one bridging oxygen, third band ($\nu_3$) at 695 $cm^{-1}$ due to the bending Vibrations of B-O-B (weak and di-borate linkage) connected with $BO_3$ and $BO_4$ structural units [23], fourth band ($\nu_4$) at 860 $cm^{-1}$ due to Stretching Vibrations B–O bond of the $BO_4$ tetrahedral units, fifth band ($\nu_5$) at 910 $cm^{-1}$ due to Stretching Vibrations of B–O–Si (Borosilicate Bridge, weak linkage) linkage units [24, 25, 26], sixth band ($\nu_6$) at 1090 $cm^{-1}$ due to Asymmetrical bending vibrations of ≡Si-O-Si≡ (strong and di-silicate linkage) associated with two $SiO_4$ structural units connected by one bridging oxygen and final band ($\nu_7$) at 1410 $cm^{-1}$ due to Symmetric stretching relaxation of the B–O band of trigonal $BO_3$ structural units [27].

Borosilicate glass exhibits energy barrier of breaking cation-oxygen-cation linkages strength sequence of Si-O-Si > B–O–Si >B-O-B depend on introduction of network modifiers like CaO, PbO, $Fe_2O_3$ and $Pr_2O_3$. By gradual increase of the mol% of $Fe_2O_3$ in the glasses the intensity of the spectral bands decreased due to structural modifications and compactness of the glass network. When increase concentrations of $Fe_2O_3$ in the glass layout, it was observed the formation of large number of NBOs indicates the variation of FTIR line intensities of these bands. In the present study content, the Ferric ($Fe^{3+}$) ions with high-spin exist in octahedral environment. The octahedral symmetry of $Fe^{3+}$ ions similar to $Pb^{2+}$ ions depolymerization in the glass network by creating more donor defects and more NBOs in glass matrices. The octahedral $Fe^{3+}$ species ($O_6$) in the glass layout the creation of maximum donor centres is expected.

Optical absorption spectra of glasses is an understanding tool, to study the Optical transition and electronic band structure of $Fe_2O_3$ (TMO) and $Pr_2O_3$ (REE) Co-doped CaO-PbO-$B_2O_3$-$SiO_2$ glasses. The strength of Ferric ions depend upon the quantitative functions of glass modifiers and glass formers in glassy environment. The Optical line intensities are increasing trend up to 0.6 mol% decrease to 0.8% and increase up to 1.0 mol% doped by $Fe_2O_3$. The intensity of optical line PrFe0.8 and the transition band strength for $^3H_4 \rightarrow {}^3P_{2, 1, 0}$, $^1D_2$, $^1G_4$, $^3F_{4, 3, 2}$ decrease due to affected by the structural compactness and change in the structure of glasses.

From the observed absorption edges, we have evaluated the optical band gaps ($E_o$) of these glasses by drawing Tauc plots between $(\alpha h\nu)^{1/2}$ and $h\nu$ as per the following equation

$$\alpha(\nu)\, h\nu = C\,(h\nu - E_o)^n \qquad \ldots\ldots\ldots (1)$$

Here the exponent (n) can take values 1/2 and 2 for indirect, direct transitions and C is a constant in glasses respectively [28]. Tauc plots for direct transition are shown in Fig.11 (a) and indirect transitions are shown in Fig.11 (b). Extrapolating the linear portion of these plots as $(\alpha h\nu)^{1/2} = 0$, $(\alpha h\nu)^2 = 0$ gives optical band gap, the theoretical band gap energy is calculated using the equation $E=hc/\lambda$. Urbach Energy ($\Delta E$) was evaluated from the slopes of the linear regions of the curves and taking their reciprocals. Urbach Energy ($\Delta E$) that indicates a measure of a disorder in glassy environment are shown in Fig.12. The cut-off wavelength ($\lambda_c$), direct and indirect band energy gaps and Urbach Energy ($\Delta E$) data is given in Table 5.

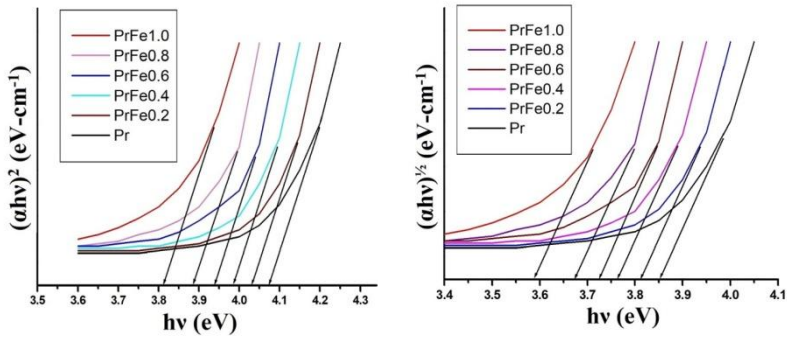


Figure 11 (a) & (b): Tauc plots to evaluate (a) direct band gap (b) Indirectband gap of CaO-PbO-$B_2O_3$- $SiO_2$: $Pr^{3+}$ / $Fe^{3+}$ Co-doped glasses

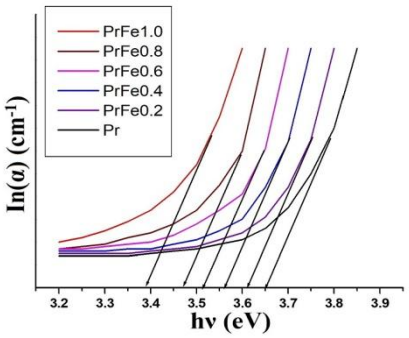


Figure 12: A plots of In(α) and h ν for CaO-PbO-$B_2O_3$-$SiO_2$: $Pr^{3+}$ / $Fe^{3+}$ Co-doped glasses

TABLE 5: The cut-off wavelength ($\lambda_c$), Optical band gaps and Urbach energy (ΔE) of CaO-PbO-$B_2O_3$-$SiO_2$: $Pr^{3+}$/$Fe^{3+}$ Co-doped glasses

| Glass Sample | Cut-off wavelength ($\lambda_c$) (nm) | Theoretical Band gap (eV) | Direct band gap (eV) | Indirect band gap (eV) | Urbach energy (ΔE) (eV) |
|---|---|---|---|---|---|
| Pr | 342 | 3.8414 | 4.0795 | 3.8522 | 0.2765 |
| PrFe0.2 | 348 | 3.8112 | 4.0343 | 3.8132 | 0.2787 |
| PrFe0.4 | 352 | 3.7789 | 3.9874 | 3.7657 | 0.2833 |
| PrFe0.6 | 356 | 3.7316 | 3.9439 | 3.7296 | 0.2869 |
| PrFe0.8 | 358 | 3.6815 | 3.8887 | 3.6752 | 0.2923 |
| PrFe1.0 | 365 | 3.5793 | 3.8167 | 3.5887 | 0.2976 |

From the Table.5it was observed that direct and indirect optical band gaps energy decreasing trend while increasing mol% of $Fe_2O_3$ content. The cut-off wavelength ($\lambda_c$) of all glass samples were shifted towards higher wavelength region in absorption spectra and at the same instant Urbach Energy (ΔE) values increasing trend with introduction of $Fe_2O_3$ was observed from Table 5.

In the present glasses, when $Fe_2O_3$ mol% is increased there is a possibility of Pb(IV) cations are replaced by Fe(III) (Ferric) ions because of these ionic radius of Ferric (78.9 pm) and Pb(IV) (79 pm) ions are almost same. The total number of $Pr^{3+}$ ($4f^2$) ion exhibits 91 microstates. $Pr_2O_3$ enters in the glass network as a modifier and $Pr^{3+}$ ions occupy intestinal positions with 6-fold coordination in the glass environment [29]. The $Fe^{3+}$ ions exhibits spin-forbidden transitions are local d-d transitions [30]. From Optical absorption spectra investigations and results the site symmetry of Ferric ions ($Fe^{3+}$) in the glass host lattice is identified as octahedral ($O_6$) site symmetry which also confirms the results of Optical studies [31]. The increasing NBOs in the glass matrices strongly influences the Optical band gap due to increasing the degree of localization of electrons there by increasing donor centres in the glass matrices, due to this reason the lowest optical band gap is observed for the glass PrFe1.0. From these glasses obviously $Fe^{3+}$ ions present and occupy interstitial positions like $Pr^{3+}$ simple ion.

The quantitatively comprehend Optical phenomena of rare earth ions in glasses, it is of great importance to evaluate radiative and non-radiative decay process of related 4f levels. The Judd-Ofelt theory is usually adopted to obtain the transition probabilities including radiative decay rate by utilizing the data of absorption cross sections of several f-f electric-dipole transitions. From the optical absorption spectra, the

calculated and experimental oscillator strengths of the absorption transitions are estimated in terms of the area under an absorption peak.

$$f_{exp} = 4.32 \times 10^{-9} \int \varepsilon(\nu)\, d\nu \quad \text{------- (2)}$$

Where ε (ν) denotes the molar extinction coefficient at a wave number ν in $cm^{-1}$.

According to the J-O theory [32, 33] the oscillator strength of electric-dipole *f-f* transition of trivalent rare earth ions from a level *(ψJ)* to a particular final state *(ψ′J′)* is given as

$$f(\psi J; \psi' J') = \frac{\upsilon}{(2j+1)} \left[\frac{8\pi^2 mc(n^2+2)^2}{3h(9n)}\right] \sum_{\lambda=2,4,6} \Omega_\lambda \langle (\psi_J \| U^\lambda \| \psi'_J)^2 \rangle \text{------- (3)}$$

where 'm' refer to the mass of the electron, 'c' is the velocity of light in vacuum, 'h' is the plank's constant, *J* and *J′* are the total angular moment of the initial and final levels, n is the refractive index of refraction of the glass, $\Omega_\lambda$ (λ=2, 4, 6) are the material parameters and $\|U_\lambda\|^2$ are the doubly reduced matrix elements of the unit tensor operator of the rank λ=2, 4 and 6. Applied J-O intensity parameters $\Omega_\lambda$ (λ=2, 4, 6) are evaluated from the least square fitting procedure using experimentally measured oscillator strength for $Pr^{3+}$ - $Fe^{3+}$ co-doped CaPbBSi glasses, the obtained values are given in Table 6. Applied J-O intensity parameters determined in the present glass network are observed to be in the trend $\Omega_4 > \Omega_6 > \Omega_2$ as shown in Table 7. The J-O parameter of $\Omega_2$ is sensitive to the symmetry of the rare-earth ion site and strongly affected by covalence between rare-earth ion and ligand ions, moreover $\Omega_4$ and $\Omega_6$ of J-O parameters are related to the rigidity of the host medium in which the ions are situated [34, 35].

TABLE 6: Theoretical and experimental oscillator strength of CaO-PbO-$B_2O_3$-$SiO_2$: $Pr^{3+}$ / $Fe^{3+}$co-doped glasses

| | GLASS SAMPLES | | | | | | | | | | | |
|---|---|---|---|---|---|---|---|---|---|---|---|---|
| Transition $^3H_4$ | Pr | | PrFe0.2 | | PrFe0.4 | | PrFe0.6 | | PrFe0.8 | | PrFe1.0 | |
| | $f_{cal}$ ($x10^{-6}$) | $f_{exp}$ ($x10^{-6}$) | $f_{cal}$ ($x10^{-6}$) | $f_{exp}$ ($x10^{-6}$) | $f_{cal}$ ($x10^{-6}$) | $f_{exp}$ ($x10^{-6}$) | $f_{cal}$ ($x10^{-6}$) | $f_{exp}$ ($x10^{-6}$) | $f_{cal}$ ($x10^{-6}$) | $f_{exp}$ ($x10^{-6}$) | $f_{cal}$ ($x10^{-6}$) | $f_{exp}$ ($x10^{-6}$) |
| $^3P_2$ | 4.8604 | 4.8673 | 4.9119 | 4.9176 | 4.9076 | 4.9055 | 4.8866 | 4.8809 | 4.5789 | 4.5762 | 4.5754 | 4.5732 |
| $^3P_1$ | 1.9814 | 1.9829 | 1.9896 | 1.9892 | 1.9875 | 1.9871 | 1.9836 | 1.9844 | 1.9802 | 1.9789 | 1.9786 | 1.9764 |
| $^3P_0$ | 2.4816 | 2.4575 | 2.5119 | 2.5134 | 2.5078 | 2.5086 | 2.4675 | 2.4652 | 2.4566 | 2.4588 | 2.4493 | 2.4485 |
| $^1D_2$ | 0.9579 | 0.9512 | 1.1311 | 1.1256 | 0.9688 | 0.9582 | 0.9618 | 0.9633 | 0.9684 | 0.9671 | 0.9520 | 0.9504 |
| $^1G_4$ | 0.2675 | 0.2641 | 0.2864 | 0.2812 | 0.2724 | 0.2703 | 0.2596 | 0.2556 | 0.2323 | 0.2298 | 0.2256 | 0.2266 |
| $^3F_4$ | 3.6117 | 3.6187 | 3.7577 | 3.7613 | 3.7311 | 3.7249 | 3.6719 | 3.6517 | 3.6319 | 3.6211 | 3.6033 | 3.6002 |
| $^3F_3$ | 4.2169 | 4.2176 | 4.4567 | 4.4316 | 4.3643 | 4.3614 | 4.2674 | 4.2532 | 4.2075 | 4.2014 | 4.1987 | 4.1963 |
| $^3F_2$ | 2.1148 | 2.1171 | 2.3952 | 2.3958 | 2.3251 | 2.3191 | 2.2314 | 2.2257 | 2.1327 | 2.1251 | 2.1081 | 2.1037 |
| Rms deviation | 0.0311 | | 0.0573 | | 0.0436 | | 0.0465 | | 0.0485 | | 0.0421 | |

TABLE 7: J-O Parameters of CaO-PbO-$B_2O_3$-$SiO_2$: $Pr^{3+}$ / $Fe^{3+}$Co-doped glasses

| Glasses Samples | $\Omega_2 x10^{-20}$ ($cm^{-2}$) | $\Omega_4 x10^{-20}$ ($cm^{-2}$) | $\Omega_6 x10^{-20}$ ($cm^{-2}$) | Trend |
|---|---|---|---|---|
| Pr | 0.74 | 4.93 | 3.64 | $\Omega_4 > \Omega_6 > \Omega_2$ |
| PrFe0.2 | 0.78 | 4.76 | 3.57 | $\Omega_4 > \Omega_6 > \Omega_2$ |
| PrFe0.4 | 0.69 | 4.71 | 3.52 | $\Omega_4 > \Omega_6 > \Omega_2$ |
| PrFe0.6 | 0.63 | 4.68 | 3.66 | $\Omega_4 > \Omega_6 > \Omega_2$ |
| PrFe0.8 | 0.59 | 4.64 | 3.61 | $\Omega_4 > \Omega_6 > \Omega_2$ |
| PrFe1.0 | 0.54 | 4.58 | 3.67 | $\Omega_4 > \Omega_6 > \Omega_2$ |

Among TM oxides, Ferric ions are versatile, because of its Optical, ESR and Photoluminescence properties are more number of potential applications of Fe contained glasses. EPR spectra position and intensities of lines depends on the paramagnetic identities contain in the glass system. The ESR signal for $Pr^{3+}$ ($4f^2$) cations is not found due to there is no electrons and no unpaired electrons in 5d orbital. Ferric oxide has ionic behaviour having both $Fe^{3+}$ (Ferric) and $O^{-2}$ (oxide) ions. Ferric ion have stable half-filled d-orbital with $3d^5$ electronic configuration has high-spin and ground state term is $^6S$ ($^6A_{1g}$ symmetry). The $d^5$ electronic configuration exhibits 252 quantum states and 16 energy levels. The Net orbital angular momentum for Ferric

ions ($3d^5$) is zero. The Ferric ions in CaPbBSPr glass environment, the excited $^4G$ term splits in four levels and assigned as $^4T_1$,$^4T_2$, $^4E$ and $^4A_1$ [ 36, 37].

Addition of $Fe_2O_3$ in the glass system, EPR spectra is observed that the high intensified resonance signals varying with $Fe_2O_3$ concentration. The high-spin of Ferric ions are also detected by ESR spectra resonance signals at g≈4.384,g≈2.00 and g≈9.37. $Fe^{3+}$ cations are strong paramagnetic character due to half-filled $3d^5$ orbital. Intensifying shoulder resonance at g≈9.37 andg≈4.384 indicates that $Fe^{3+}$ ions occupy octahedral symmetry ($O_6$). From the EPR spectra analysis of glasses indicates the highest covalence environment for 1 mol% of $Fe^{3+}$ ions in the glass system. The most familiar oxidation of iron exist stable valence of $Fe^{3+}$ ions in borosilicate glasses with octahedral symmetry ($O_6$). Introducing $Fe^{3+}$ ions in the glass network acts as probe in the borosilicate glass network.

The resonance signals at g≈4.384 and g≈9.37 originates from paramagnetic resonance signals of isolated half-filled $Fe^{3+}$ ions strongly occupied in octahedral sites with oxygen ligands [38, 39]. The EPR spectra of $Fe^{3+}$ ions exhibit resonance signals at g≈4.384 and g≈9.37 arise from the isotropic transition within the Kramer's doublets [40, 41]. The resonance intensity signal at g≈2.0 weak signal due to spin-spin interactions.

Photoluminescence spectra (PL) is conventional technical tool for identifying radiative and non-radiative emission transitions in the glass system. In order to understand the photoluminescence properties of $Fe^{3+}$ ions, the Tanabe-Sugano (T-S) diagram for stable half-filled $3d^5$ electronic configuration should be considered. The emission transitions of $Fe^{3+}$ ions is generally originated between 680 and 740 nm (1.82 – 1.67 eV) depending upon the glass composition and this emission transition occurs from a spin-forbidden$^4T_{2g}$ ($^4G$)→$^6A_{1g}$ ($^6S$) transition within the stable half-filled $3d^5$ electrons of the ion [ 42, 43]. The emission transitions of $^4T_{2g}$ ($^4G$) →$^6A_{1g}$ ($^6S$) with Ferric ions ($Fe^{3+}$) are the non-radiative in the glass system [44, 45]

From PL spectra the hyper intensity of $^3P_0$→$^3F_2$ emission transition of $Pr^{3+}$ ions spectral overlaps with $^4T_{2g}$ ($^4G$) →$^6A_{1g}$ ($^6S$) transition of $Fe^{3+}$ ions, since there is a chance of non-radiative energy transfer through multi-pole interaction. The significant high intense emission transition of $Pr^{3+}$ ion through the addition of $Fe^{3+}$ ion suggests that $^3P_0$→$^3F_2$ level of $Pr^{3+}$ ions are populated due to energy transfer from $Fe^{3+}$ ions ($Fe^{3+}$→$Pr^{3+}$). In this view of contribution of $Pr^{3+}$ ion emission transition $^3P_0$→$^3F_2$ was the bright red emission was observed [46]. The luminescence mechanism, the excitation of $Pr^{3+}$ ion to $^3P_2$ energy level, a non-radiative de-excitation progressed from $^3P_2$ to $^3P_{1,0}$ and $^1D_2$ energy levels at finally the photon energy emission takes place from $^3P_{1,0}$ and $^1D_2$ energy levels to lower laying levels. Hence, the intense de-excitation are mainly arise from $^3P_0$ and $^1D_2$ excited energy levels are presented in Fig.13.The energy level diagram including absorption and emission transitions of $Pr^{3+}$ - $Fe^{3+}$ ions Co-doped CaPbBSi glasses. Applied J-O parameters, β (Branching ratio) of bright red emission due to $^3P_0$→$^3F_2$ (1.75 eV) transition is evaluated in Table8.

TABLE 8: Various radiative properties of CaO-PbO-$B_2O_3$-$SiO_2$ : $Pr^{3+}$ / $Fe^{3+}$ Co-doped glasses

| Transitions | GLASS SAMPLES | | | | | | | | | | | |
|---|---|---|---|---|---|---|---|---|---|---|---|---|
| | Pr | | PrFe0.2 | | PrFe0.4 | | PrFe0.6 | | PrFe0.8 | | PrFe1.0 | |
| | $A(s^{-1})$ | β% | $A(s^{-1})$ | β% | $A(s^{-1})$ | β% | $A(s^{-1})$ | β% | $A(s^{-1})$ | β% | $A(s^{-1})$ | β% |
| $^3P_0$→$^3H_4$ | 512 | 5.79 | 530 | 5.95 | 522 | 5.81 | 514 | 5.31 | 503 | 5.21 | 476 | 5.11 |
| $^3P_1$→$^3H_5$ | 609 | 6.51 | 701 | 7.12 | 698 | 6.76 | 672 | 6.47 | 641 | 6.32 | 593 | 6.17 |
| $^3P_0$→$^3H_5$ | 918 | 11.67 | 1012 | 11.91 | 1001 | 11.77 | 971 | 10.71 | 934 | 10.55 | 906 | 10.21 |
| $^1D_2$→$^3H_4$ | 2326 | 14.19 | 2418 | 15.11 | 2396 | 14.55 | 2346 | 14.31 | 2291 | 13.76 | 2259 | 13.69 |
| $^3P_0$→$^3H_6$ | 2749 | 42.55 | 2842 | 45.78 | 2813 | 44.13 | 2751 | 43.13 | 2731 | 41.76 | 2715 | 40.36 |
| $^3P_0$→$^3F_2$ | 3156 | 51.23 | 3174 | 52.09 | 3156 | 51.76 | 3144 | 51.53 | 2897 | 42.11 | 3158 | 54.26 |
| $^3P_1$→$^3F_3$ | 1408 | 17.62 | 1692 | 18.45 | 1603 | 17.86 | 1534 | 17.02 | 1421 | 16.81 | 1376 | 16.54 |
| $A_T$ ($s^{-1}$) | 7441.36 | | 8073.91 | | 7341.76 | | 7311.44 | | 5114.76 | | 7204.01 | |

The highest Branching ratio (β) value for glass PrFe1.0 compared for all the prepared glasses. From the present content observation suggests that 1.0 mol% of $Fe_2O_3$ is high optimization concentration in present glass matrix to originated high luminescent efficiency. The energy transfer mechanism nature between $Fe^{3+}$→$Pr^{3+}$ suggests electric dipole-dipole in glass environment. The large value of energy transfer probabilities and transfer efficiencies suggests that $Fe^{3+}$ ions acts as a good sensitizer (TM) for $Pr^{3+}$ activator (RE) ions in calcium lead borosilicate glasses.

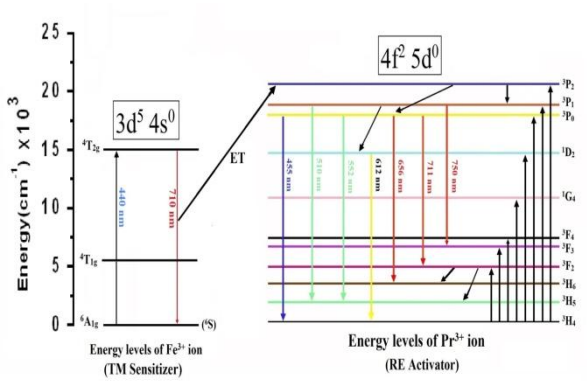


Figure 13: Energy level diagram of CaO-PbO-$B_2O_3$-$SiO_2$ : $Pr^{3+}$/ $Fe^{3+}$ Co-doped glasses

CIE chromaticity coordinates for all co-doped glass samples are evaluated and results are listed in Table.9shown in Fig.14. The emitting color of the glasses is in red with increasing mol% of $Fe_2O_3$ content. Particularly the CIE chromaticity coordinates for PrFe1.0 is in Bright red with 1.75 eV.

TABLE 9: The Color coordinates of CaO-PbO-$B_2O_3$-$SiO_2$: $Pr^{3+}$/ $Fe^{3+}$Co-doped glasses

| Glasses Samples | X | Y |
|---|---|---|
| Pr | 0.63187 | 0.31156 |
| PrFe0.2 | 0.64324 | 0.30877 |
| PrFe0.4 | 0.64831 | 0.30042 |
| PrFe0.6 | 0.65684 | 0.29318 |
| PrFe0.8 | 0.65716 | 0.28225 |
| PrFe1.0 | 0.66143 | 0.27189 |

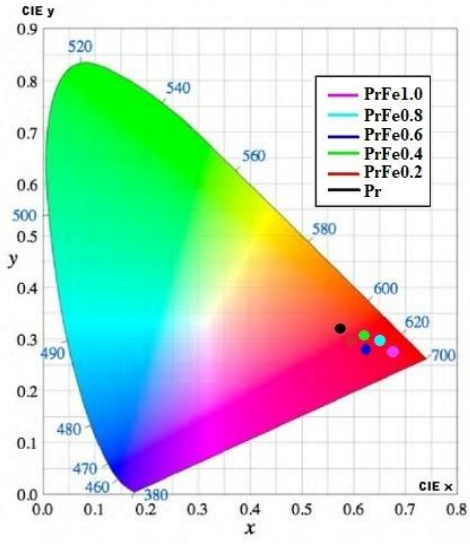


Figure 14: The color space chromaticity diagram of CaO-PbO-$B_2O_3$-$SiO_2$ : $Pr^{3+}$/ $Fe^{3+}$Co-doped glasses

## VI. Conclusion

A novel series of CaO - PbO - $B_2O_3$ - $SiO_2$ glasses were Co-doped with $Pr_2O_3$ and $Fe_2O_3$ by conventional melt-quenching process. The glasses were characterized by XRD, FTIR, Optical Absorption, EPR and Photoluminescence spectra. The main conclusion of this paper are as follows:

1. Physical parameters of all glasses are evaluated. The density and refractive index of all the studied glasses were strongly influenced the changes in the structure of glasses, structural compactness and increasing non-bridging oxygen atoms (NBOs) with increasing $Fe_2O_3$ content.

2. The Optical basicity increases with $Fe_2O_3$ mol% indicating high-rich electron donor ability of oxide ion ($O^{2-}$) in the glass environment is studied in the glasses, while molar refractivity is reverse trend with average molecular weight.
3. From the study of XRD spectra indicates that all the glasses are in amorphous nature. DTA measurements of all the glasses reveal PrFe1.0 glass is highly stable against devitrification.
4. FTIR studies revels the presence of $SiO_4$, $BO_4$ and $BO_3$ local structural frequencies in calcium lead borosilicate glasses Co-doped with $Pr_2O_3$ and $Fe_2O_3$.
5. The cut-off wavelength ($\lambda_c$), direct and indirect band gaps energy values are evaluated. The lower value of optical band gap of PrFe1.0 indicates higher degrees of disorder of this glass.
6. In the present paper Optical absorption spectra and Luminescence spectra were characterized by applied Judd-Ofelt theory.
7. From the Photoluminescence spectra by co-doping of $Fe^{3+}$ - $Pr^{3+}$ ions, it is observed that $^3P_0 \rightarrow {}^3F_2$ significant notable transition falls in bright red region at 711 nm (1.75 eV) due to energy transfer from $^4T_{2g}$ ($^4G$) $\rightarrow {}^6A_{1g}$ ($^6S$) transition of $Fe^{3+}$ ions to $^3P_0 \rightarrow {}^3F_2$ levels of $Pr^{3+}$ ions.
8. From the Optical absorption and Photoluminescence spectra confirmed the $Fe^{3+}$ ions occupy higher coordination of 6-fold octahedral ($O_6$) symmetry in these Co-doped glasses.
9. The EPR spectra studied all the results of that prepared glasses exhibited strong intense resonance signals. Which indicates isolated $Fe^{3+}$ ions attributed octahedral symmetry ($O_6$) with stable half-filled $3d^5$ electronic configuration by high-spin of unpaired electrons.
10. From CIE chromaticity coordinates, it was found that PrFe1.0 glass fall in Bright red. The PrFe1.0 glass have high potential advanced technological applications in red LED, bright visible red lasers, red LED sensors, tunable solid state red lasers, Optical components and fiber optic communications.

## References


[1]. Jantzen, C.M. J. Non-Cryst. Solids, 1986, 84, 215.
[2]. Cao, H., J. W. &Kalb, P.D. Brookhaven National Laboratory Annual Report-52595, 1995.
[3]. Kaky, Kawa M., M. l. Sayyed, Farah Laariedh, Alyaa H. Abdalsalam, H.O. Tekin, and S. O. Baki, Applied Physics A125, no.1 (2019): 1-12.
[4]. Sayyed, M.l., Ali A. Ati, M. H. A Mhareb, K. A. Mahmoud, Kawa M. Kaky, S. O. Baki, and M. A. Mahdi, Journal of Alloys and Compounds 844 (2020): 155668.
[5]. El-Mallawany, Raouf A. H. Tellurite Glasses Handbook. CRC Press, Boca Raton, LLC, Florida, USA, 2002.
[6]. Downing, E., Hesselink, L., Ralston, J., and Macfarlane, R.A., 1996, three-color, solid-state, three dimensional display Science, vol.45 pp.45.
[7]. Y.N. Ch. Ravi Babu, P. Sree Ram Naik, K. Vijaya Kumar. N. Rajesh, A. Suresh Kumar, Journal of Quantitative Spectroscopy and Radiative Transfer, 113 [13] 920120 1669-1675.
[8]. Adel, A.; Farag, M.; El-Okr, M.; Elrasasi, T.; El-Maansy, M. Egypt. J. Chem. 2020, 63, 2-3.
[9]. El-Alaily, N.; Sallam, O.; EZZ-Eldin, F, J. Non-Crystalline Solids 2019, 523,119604.
[10]. Kassab, L.R.P.; de Araujo, C.B. Linear and nonlinear optical properties of some tellurium oxide glasses. In Technological Advances in Tellurite Glasses: Properties, processing and Applications: Rivera, V.A.G., Manzani, D., Eds.; Springer: Cham, Switzerland, 2017; Chapter 2; pp.15-39.
[11]. M. Jamnicky, P. Znasic, D. Tunega, M.D. Ingram, J. Non-Cryst. Solids 185 (1995) 151–158.
[12]. N.J. Cherepy, D.B. Liston, J.A. Lovejoy, H. Deng, J.Z. Zhang, J. Phys. Chem. B 102 (1998) 770–776.
[13]. J. E. Shelby, M. Lopes. 2005. Introduction to glass science and technology, 2nd ed., The Royal Society of Chemistry, Cambridge.
[14]. Danilo Manzani, David Paboeuf, Philippe Goldner, Fabien Bretenaker, Opt. Mater. 35(2013) 383–386.
[15]. P. Vijaya Lakshmi, T. Sambasiva Rao, K. Neeraja, D.V. Krishna Reddy, N. Veeraiah, M. Rami Reddy, Journal of Luminescence 190 (2017) 379–385.
[16]. V. Naresh and S. Buddhudu, Ferroelectrics, 437:110-125, 2012.
[17]. M. Lenglet, F. Hochu, Z. Simsa, Mater. Res. Bull. 33 (1998) 1821–1833.
[18]. Essam A. Elkelany, Moukhtar A. Hassan, A. Samir, A.M. Abdel-Ghany, H. H. El-Bahnasawy, M. Farouk, Optical Materials 112 (2021) 110744.
[19]. Amit Kumar Prasad, Mayank Jain, Journal of Luminescence 196 (2018) 462-469.
[20]. R. P. SreekanthChandradhar, B. Yasoda, J.L. Rao, J. Non-Cryst. Solids 353 (2007) 2355-2362.
[21]. G. Naga Raju, M. Srinivasa Reddy, K.S.V Sudhakar, N. Veeraish, Opt. Mater. 29 (2007) 1467-1474.
[22]. K.K. Mahato, Anitha Rai, S.B. Rai, Spectrochim. Acta Part A 70 (2008) 577-586.
[23]. H. Doweidar, Yasser B. Saddeek, J. Non-Cryst. Solids 355 (2009) 348-354.
[24]. T.G.V.M. Rao, A. Rupesh Kumar, K. Neeraja, N. Veeraiah, M. Rami Reddy, J. Alloy. Compd. 557(2013)209-217.
[25]. Y. Lai, Y. Zeng, X. Tang, H. Zhang, Z. Han, H. Su, RSC Adv. 6 (96) (2016) 93722-97728.
[26]. C. Gautam, A.K. Yadav, V. K. Mishra, K. Vikram, 2 (4) (2012) 47-54.
[27]. J. Zhong, X. Ma, H. Lu, X. Wang, S. Zhang, W. Xiang, J. Alloy. Compd. 607 (2014) 177-182.
[28]. Davis, E. A., Philos. Mag. 22 (1970) 903-922.
[29]. Shelby J E 1994 Key Eng. Mater. 94 43.
[30]. R.G. Burns, Mineralogical Applications of Crystal Field Theory, 1993.
[31]. Devaraja P.B., Avadhani D.N., Nagabhushana H., Prashantha S.C., Nagabhushana B.M., Nageswaupa H.P., Prasad D.B., J. Radiat. Res. Appl. Sci., 8 (2015) 362.
[32]. B. R. Judd, Phys. Rev. 127 (1962) 750-755
[33]. G.S. Ofelt, J. Chem. Phys. 37 (1962) 511-514.
[34]. Sk. Mahamuda, K. Swapna, A. Srinivasa Rao, T. Sasikala, L. Rama Moorthy, Physica B 428 (2013) 36-42.
[35]. M.V. Vijaya Kumar, V. Lokeswara Reddy, N. SoorajHussian, B.C. Jamalaiah, J. Non-Cryst. Solids 364 (2013) 20-27.

[36]. Furdyna, J. K. Diluted Magnetic Semiconductors, J. Appl. Phys. 1988, 64, R29-R64.
[37]. R. Heitz, P. Maxim, L. Eckey, P. Thurian, A. Hoffmann, I. Broser, K. Pressel and B.K. Meyer, Phys. Rev. B55, 4382 (1997).
[38]. P. S. Rao, S. Subramanian, Mol. Phys. 54 (1985) 415-427.
[39]. P. Sambasiva Rao. Spectrochim. Acta A 52 (1996) 1127-1134.
[40]. A. Abragam. B. Button, in: Electron Paramagnetic Resonance of Transition Ions, Clarendon, Oxford, 1970 p.203.
[41]. J.R. Pilbrow, in: Transition Ion Electron Paramagnetic Resonance, Clarendon Oxford, 1990 p. 135.
[42]. M.R. Krbetschek, J. Götze, A. Dietrich, T. Trautmann, Spectral information from minerals relevant for luminescence dating, Radiat. Meas. 27 (5) (1997) 695–748.
[43]. N.R.J. Poolton, L. Bøtter-Jensen, O. Johnsen, Radiat. Meas. 26 (1) (1996) 93–101.
[44]. I. Fontana, A. Lauria and G. Spinolo, Phys. Status Solidi B, vol. 244, no. 12, pp. 4559-4677.
[45]. P. Köhler and G. Amthauer, J.Solid State Chem., vol. 28, no.3, pp. 329-343.
[46]. M. Venkateswarlu, M.V.V.K.S. Prasad, K. Swapna, Sk. Mahamuda, A. Srinivasa Rao, A. Mohan Babu, D. Haranath, J. Ceramics International 40 (2014) 6261-6269.

K. Kalyan Chakravarthi, et. al. "1.75 eV Bright Red Emission of $Pr^{3+}$ ions doped in CaO-PbO-$B_2O_3$-$SiO_2$ glasses by $Fe^{3+}$ sensitizer ions for red laser and LED."*International Journal of Engineering Science Invention (IJESI)*, Vol. 11(08), 2022, PP 34-48.Journal DOI- 10.35629/6734